This article has been accepted for publication in IEEE Internet of Things Journal. This is the author's version which has not been fully edited and content may change prior to final publication. Citation information: DOI 10.1109/JIOT.2025.3530866

AoA and RSSI-Based BLE Indoor Positioning System with Kalman Filter and Data Fusion

Andrey Fabris, Ohara Kerusauskas Rayel, João Luiz Rebelatto, *Senior Member, IEEE*, Guilherme Luiz Moritz, Richard Demo Souza, *Senior Member, IEEE*.

***Abstract*—This work aims at improving indoor positioning systems (IPS) by integrating multiple radio frequency techniques, namely Received Signal Strength Indication (RSSI), Angle of Arrival (AoA), and a combination of both, within the Bluetooth Low Energy (BLE) 5.1 framework. While AoA stands out for its precision, low energy consumption, and cost-effectiveness, RSSI is characterized by its simplicity and widespread availability. By resorting to a database of real RSSI and AoA measurements from a BLE 5.1 target node in a 14×8-meter environment, our work employs the Kalman Filter (KF) to improve the accuracy of multilateration, AoA combined with RSSI, and AoA-only algorithms. Moreover, we consider one more step in our IPS where the aforementioned KF-filtered outputs are then fused through a track fusion model. Results demonstrate that the proposed scheme, which we refer to as Angle-RSSI Fusion Localization (ARFL), significantly improves localization accuracy compared to other techniques. In particular, it reduces up to 81.61% in the average position error when compared to multilateration with KF. This advanced IPS offers a cost-effective and precise solution suitable for various applications in industries such as healthcare, commerce, and logistics.**

***Index Terms*—Angle-of-Arrival, Bluetooth Low Energy, Indoor Positioning System, Kalman Filtering, Sensor Fusion.**

I. Introduction

Indoor Positioning System (IPS) are essential for providing accurate location tracking in environments where traditional GPS signals are not available or unreliable, such as inside buildings [1]. These systems are particularly valuable in industries such as retail, healthcare, manufacturing, and logistics, where precise tracking improves operational efficiency, safety, and customer experience [2], [3].

Despite their usefulness, common IPS methods such as the Received Signal Strength Indication (RSSI), Angle of Arrival (AoA), Time of Arrival (ToA) and Time Difference of Arrival (TDoA) face significant challenges, including signal interference and multipath effects, which degrade accuracy in real-world environments [4]. Additionally, there is a constant trade-off between energy consumption and system performance, especially for battery-powered devices, which affects system usability and user satisfaction [5].

To address these challenges, we propose a hybrid Bluetooth Low Energy (BLE)-based localization method that fuses RSSI and AoA measurements using a sensor fusion technique based on Kalman Filter (KF) [6]. By integrating multiple positioning methods such as multilateration and triangulation, the proposed approach improves accuracy in indoor environments where signal distortion and interference are common.

This work is validated using the dataset from Girolami et al. [7], which includes RSSI and AoA measurements collected in various scenarios. We compare the performance of our proposed Angle-RSSI Fusion Localization (ARFL) method against traditional RSSI-based and AoA-based approaches, showing the superiority of ARFL under several error metrics.

The rest of this paper is as follows: Section II presents the literature review, and Section III describes the system model and Bluetooth Direction Finding (DF) technology. The proposed sensor fusion-aided scheme is presented in Section IV, while Section V analyzes numerical results. Finally, Section VI concludes the paper and discusses some future works.

II. BLE-based IPS: Literature Review

The introduction of DF in BLE 5.1 [5] has allowed devices to determine the direction of a BLE signal. This new feature, maintained in recent BLE versions, has led to increased research into methods and algorithms for IPS. In [8], the authors consider BLE 5.1 devices based on AoA to estimate the position of static targets, moving nodes, as well as proximity detection scenarios. They also evaluate the influence of frequency channels and human posture. However, the aforementioned work uses only one anchor (a BLE device equipped with an antenna array). Compared to traditional RSSI-based approaches, the results show that the estimated AoA values are less prone to fluctuations than RSSI under stationary conditions. Furthermore, the results present errors ranging from $1.82\,\mathrm{m}$ to $1.90\,\mathrm{m}$ in the static positioning scenario, while for the mobility scenario, the 75th percentile is $2.78\,\mathrm{m}$. Regarding the proximity scenario, the algorithm correctly identifies proximity with an accuracy of 93%.

The same authors from [8] also provide in [7] a BLE 5.1-based data collection specifically designed for indoor localization (available for download in [14]), and describe the methodology and technical details required to reproduce the experiments reported in the aforementioned work. The authors also evaluated the behavior of RSSI across different channels

A. Fabris, O.K. Rayel and G.L. Moritz are with the PPGSE, UTFPR, Curitiba-PR, 80230-901, Brazil; andreyfabris@alunos.utfpr.edu.br, {oharakr, moritz}@utfpr.edu.br

J.L. Rebelatto is with the CPGEI, UTFPR, Curitiba-PR, 80230-901, Brazil; jlrebelatto@utfpr.edu.br

R.D. Souza is with the PPGEEL, UFSC, Florianópolis-SC, 88040-900, Brazil; richard.demo@ufsc.br

This work was supported by Agência Nacional de Energia Elétrica and Celesc Distribuição S.A. (PD05697-1323/2023), CNPq (305021/2021-4, 307222/2023-3, 402378/2021-0, 403124/2023-9), RNP/MCTIC 6G Mobile Communications Systems (01245.010604/2020-14) and Fapemig Ciência por Elas (APQ-04523-23).

TABLE I: Summary of some AoA-related positioning systems.

Reference	HW/SW (Detail)	# Anchors	Method	In/Outdoor	AoA Error [°]	Pos. Error [m]	Mobility
[8]	HW (XPLR-AOA-1)	1	Trigonometry	Indoor ($13.8 \times 8\,\mathrm{m}$)	$5°$	1.82	Static, Mobility, Proximity
[7]	HW (XPLR-AOA-1)	4	Trigonometry	Indoor ($13.8 \times 8\,\mathrm{m}$)	$5°$	N/A	Calibration, Static, Mobility, Proximity
[9]	Simulation	4	Triangulation	Indoor ($12 \times 6\,\mathrm{m}$)	$5°$	0.59	Static
[10]	HW (CC26X2R + BOOSTXL-AOA)	2	Triangulation	Indoor ($5 \times 5\,\mathrm{m}$)	$1.83°$	0.36	Static
				Outdoor ($5 \times 5\,\mathrm{m}$)	$0.48°$	0.22	Static
[11]	HW (NRF52833)	1	Trigonometry	Indoor ($4.8 \times 4.8\,\mathrm{m}$)	$5°$	0.7	Static
[12]	HW (CC2530)	4	Hybrid AoA-RSSI	Indoor ($10 \times 9\,\mathrm{m}$)	N/A	0.45	Mobility
[13]	HW (USRP X310 + B205mini-i)	2	Triangulation	Indoor ($6 \times 3\,\mathrm{m}$)	$2°$	0.14	Static

and AoA in different scenarios, focusing on AoA results and accuracy in a 14×8-meter environment.

Other authors have also made datasets available from different environments, including simulations, to support the research and development of BLE-based IPS algorithms. In [15], a dataset of measurements (along with the Python code to manipulate the dataset) was generated through a simulation process based on a mathematical model. Another work with a dataset available is [16] (data set available in [17]), where four BLE anchors were mounted in a $100\,\mathrm{m}^2$ room.

To shed some light on optimal antenna locations for localization purposes, the work in [9] presents the characteristics of AoA-aided BLE 5.1 DF starting from a comparison to commonly adopted RSSI-based trilateration. It also evaluates the confidence region resulting from a trilateration-based approach, assuming the absolute error of $5°$ reported by the u-blox XPLR-AOA-1 datasheet [18]. As a result, the authors show that the shape of the confidence regions changes to irregular polygons, making it possible to determine the contribution of each anchor in the position estimation. To evaluate the impact of the number of BLE beacons in IPS, the authors in [19] performed simulations showing that the number and proximity of these devices leads to a more accurate position estimate. However, there is a limit where the increase in BLE beacons does not reflect an effective improvement in error.

In addition, [10] and [20] compare the indoor and outdoor accuracy of an AoA-based positioning system, showing that both the average angular error and the associated position estimate are more accurate outdoors due to the reduced multipath effect present in outdoor spaces compared to indoor spaces.

The precision of the trilateration method with BLE beacons is studied in [21], where the authors consider three BLE beacons and one mobile phone measuring the RSSI in a $92\,\mathrm{m}^2$ room, divided into 163 measurement points. The results indicate a mean distance error of $7.97\,\mathrm{m}$ with an average of ten measurements at each position. To enhance accuracy, an IPS based on track-to-track fusion (T2TF) with fingerprinting and multilateration is proposed in [22]. With four anchors in a 3×3-meter room, an average error of $1.6\,\mathrm{m}$ is obtained. The authors also show that the average error decreases as the number of BLE anchors increases.

In the scope of AoA-based methods, the results of RSSI, AoA, and Pedestrian Dead Reckoning (PDR) frameworks are evaluated in [23]. The authors also propose a fusion method based on reinforcement learning (RL). In all of the considered scenarios, the results demonstrate that AoA has better accuracy than the other two techniques, whilst the fusion method improves the results. In [24], a simulation set-up is provided in which mobile receivers are equipped with BLE 5.1 antenna arrays, while the fixed infrastructure consists of battery-powered beacons. Considering a real-world data set of AoA measurements, their simulator suggests that sub-meter accuracy can be achieved using one beacon per $15\,\mathrm{m}^2$ and a beacon transmission period of $500\,\mathrm{ms}$. Finally, the work in [25] demonstrates that the Root Mean Squared Error (RMSE) in the azimuth angle is lower when the AoA is less than $30°$, and the error increases as the angle increases. Furthermore, Table I compares some AoA-based IPS papers.

Against this background, this work aims to evaluate the influence of sensor fusion on the accuracy of an RSSI and AoA-based IPS. More specifically, we develop a framework in which multiple KFs are used in RSSI and AoA measurement datasets from [7], whose outputs are combined by means of the sensor fusion technique. This work's main contribution is the introduction of a novel variation of the T2TF technique, where the outputs of Kalman-filtered BLE IPS based on AoA and RSSI are integrated. Most IPS approaches fuse estimates derived from the same measurements across standalone networks, such as WLAN and GSM, or combine distinct measurements from different sources, like RSSI from a WLAN and PDR from an Inertial Navigation System (INS) [1]. To the best of the authors' knowledge, the application of such variation of the T2TF technique to real measurements obtained from different aspects of a single received signal within a BLE framework has not been addressed elsewhere. Multilateration, trigonometry with RSSI and AoA, and triangulation methods were selected for their real-time applicability in any environment. Additionally, unlike fingerprinting, these methods do not require the creation of a new RSSI database for possible target positions in response to room changes, nor do they pose great difficulty adapting to environmental changes. They also do not demand an extensive training phase or powerful hardware for implementing advanced machine learning techniques.

Notation: Throughout this paper, lowercase and uppercase boldface letters refer, respectively, to vectors and matrices, with $\mathbf{A}^T$ and $\mathbf{A}^{-1}$ being the transpose and inverse of matrix $\mathbf{A}$, respectively. Moreover, $c \sim \mathcal{N}(a, b)$ represents a normal distributed random variable c with average a and variance b. Positions in 2D coordinates are represented by $\begin{bmatrix} x & y \end{bmatrix}^T$.

III. System Model and Preliminaries

This work considers a $112\,\mathrm{m}^2$ room, where the Region of Interest (RoI) is rectangular with 12×6 meters. The RoI has four anchors, with the n-th anchor placed at known coordinates

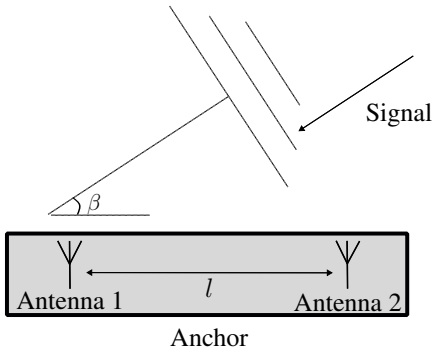

Fig. 1: Illustration of AoA.

$\begin{bmatrix} x_n & y_n \end{bmatrix}^T \in$ RoI for $n \in \{1, \ldots, 4\}$. The aim is to estimate the 2D trajectory of a BLE tag with positions $\begin{bmatrix} x_{\text{tag}} & y_{\text{tag}} \end{bmatrix}^T$ under constant velocity motion over a total test duration of K steps, using RSSI and AoA measurements from the anchors, by processing the data packets sent by the BLE tag.

A. Bluetooth 5.1 Direction Finding (BLE-DF)

The BLE-DF specification presented in [5] outlines that version 5.1 of Bluetooth can estimate the direction of a battery-powered tag based on the phase shift of the signal received by two or more antennas. More specifically, the specification states that a Constant Tone Extension (CTE) is supplemented to a BLE packet, allowing an anchor to obtain in-phase and quadrature (IQ) data from the signal, information that can be used to estimate the AoA of the received packet. The details of the update to the specification [5] are discussed in [26].

In a BLE 5.1-based localization system, the tag advertises BLE beacons with an additional field that comes after the Cyclic Redundancy Check (CRC) code, the aforementioned CTE, which consists of a radio frequency sinusoidal signal modulated by a constant series of consecutive ones. Throughout the CTE part of the BLE packet, the anchor can extract the phase difference (ψ) between the signals received from each antenna in the array. Given the wavelength (λ) of the signal and the distance (l) between the antennas, the anchor can calculate the AoA (β) of the signal as

$$\beta = \arccos\left(\frac{\psi\lambda}{2\pi l}\right), \tag{1}$$

which is illustrated in Fig. 1. However, when taking into account multipath reception, signal spread delay, and noise, it is necessary to adopt more reliable methods to calculate the AoA, such as Multiple Signal Classification (MUSIC) [26].

BLE-DF uses uniform circular arrays (UCAs) and uniform rectangular arrays (URAs) to achieve an estimation of elevation and azimuth angles. Fig. 2 illustrates the azimuth (θ) and elevation (ϕ) angles obtained by the u-blox C211 antenna array. This hardware calculates both angles within the range of $-90°$ to $90°$ [27]. The azimuth is the angle between the x-axis and the orthogonal projection of the vector $\overline{\text{AT}}$ onto the xy-plane. It is positive when measured from the positive x-axis to the negative y-axis and negative from the positive x-axis to the positive y-axis. The elevation is the angle between the vector $\overline{\text{AT}}$ and its orthogonal projection onto the xy-plane.

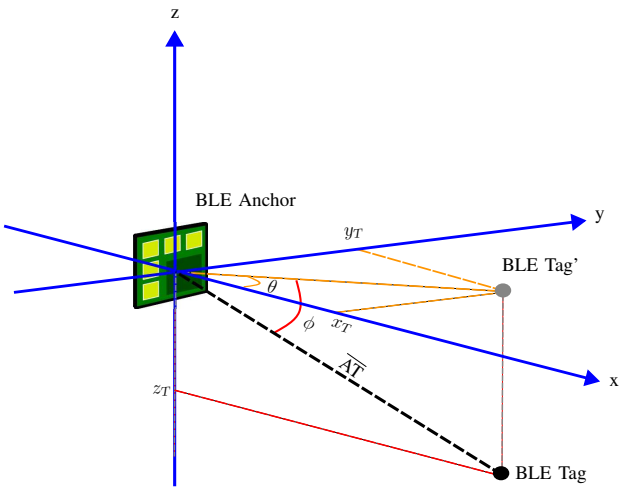

Fig. 2: Illustration of a BLE tag in the 3D plane, its projection in the xy plane, and the AoAs from DF.

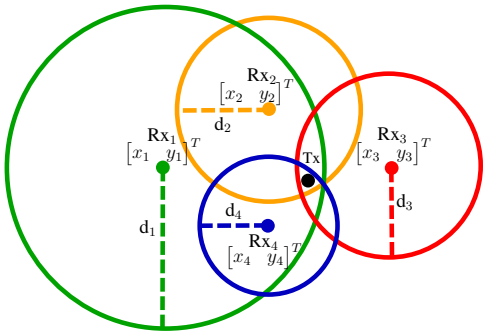

Fig. 3: Multilateration example: The colored dots represent the BLE anchor nodes, while the black dot at the intersection point represents the BLE tag.

It is positive from the positive xy-plane towards the positive z-axis and negative when measured from the positive xy-plane towards the negative z-axis [27]. Given these definitions, the azimuth and elevation angles represented in Fig. 2 are negative.

1) Multilateration: Multilateration is a technique used to determine the location of an object by measuring its distances from multiple known receiving devices [28]. In BLE-based systems, RSSI values measured from BLE received packets can be used to estimate the distance between the anchor and the tag. Fig. 3 illustrates the concept of multilateration. Here, the anchors Rx_n have known coordinates denoted as $\begin{bmatrix} x_n & y_n \end{bmatrix}^T$, for $n \in \{1, 2, 3, 4\}$. Furthermore, d_n represents the distance between the anchor Rx_n and the BLE tag. The position of the target is then estimated to be at the intersection of circles whose radii are the distances to the tag.

The RSSI at the n-th anchor, given the distance d_n, can be estimated using a log-normal propagation model as [29]

$$\text{RSSI}_{d_n} = \text{RSSI}_{d_0} - 10\alpha \log_{10}\left(\frac{d_n}{d_0}\right) + \mathcal{X}_\sigma, \tag{2}$$

where RSSI_{d_n} is the RSSI (in dBm) at distance d_n, RSSI_{d_0} is the RSSI at reference distance d_0, α is the path-loss coefficient (PLc), and $\mathcal{X}_\sigma \sim \mathcal{N}(0, \sigma^2)$ models the shadowing (dB). Since the shadowing has $0\,\text{dB}$ mean, upon averaging the RSSI of

several packets sent by a BLE tag, the distance between the anchor and the tag can be estimated by rearranging the terms of (2) as follows:

$$\hat{d}_n = d_0\, 10^{\frac{\text{RSSI}_{d_0} - \text{RSSI}_{d_n}}{10\alpha}}. \tag{3}$$

After estimating the distance between the BLE tag and each anchor from (3), multiple distance estimates can be used to determine the tag position. Consider that the relationship between a BLE tag placed in coordinate $\begin{bmatrix} x_{\text{tag}} & y_{\text{tag}} \end{bmatrix}^T$ and its distance to the n-th anchor is given by $d_n = \sqrt{(x_{\text{tag}} - x_n)^2 + (y_{\text{tag}} - y_n)^2}$. Assuming that $\hat{d}_n \simeq d_n$, by squaring and subtracting the N-th equation from the n-th equation, and rearranging the terms, one obtains a linear function of x_{tag} and y_{tag} as in [30]:

$$\begin{aligned} -x_n^2 - y_n^2 + x_N^2 + y_N^2 + (\hat{d}_n)^2 - (\hat{d}_N)^2 = \\ x_{\text{tag}}(-2x_n + 2x_N) + y_{\text{tag}}(-2y_n + 2y_N). \end{aligned} \tag{4}$$

By expanding (4) in terms of n for N anchors, a linear system is obtained, which can be expressed in matrix form as $\mathbf{b} = \mathbf{M}\mathbf{p}$, where:

$$\mathbf{b} = \begin{bmatrix} -x_1^2 - y_1^2 + x_N^2 + y_N^2 + (\hat{d}_1)^2 - (\hat{d}_N)^2 \\ -x_2^2 - y_2^2 + x_N^2 + y_N^2 + (\hat{d}_2)^2 - (\hat{d}_N)^2 \\ \vdots \\ -x_{N-1}^2 - y_{N-1}^2 + x_N^2 + y_N^2 + (\hat{d}_{N-1})^2 - (\hat{d}_N)^2 \end{bmatrix}, \tag{5}$$

$$\mathbf{M} = \begin{bmatrix} -2x_1 + 2x_N & -2y_1 + 2y_N \\ -2x_2 + 2x_N & -2y_2 + 2y_N \\ \vdots & \vdots \\ -2x_{N-1} + 2x_N & -2y_{N-1} + 2y_N \end{bmatrix}, \text{ and} \tag{6}$$

$$\mathbf{p} = \begin{bmatrix} x_{\text{tag}} \\ y_{\text{tag}} \end{bmatrix}. \tag{7}$$

Due to the errors in $\{\hat{d}_n\}_{n=1}^N$ caused by shadowing effects, a least squares method is used to minimize $\sum_{n=1}^N (d_n - \hat{d}_n)^2$ and estimate the coordinates of the BLE tag as $\hat{\mathbf{p}}_{\text{MLT}} = \hat{\mathbf{p}} = (\mathbf{M}^T\mathbf{M})^{-1}\mathbf{M}^T\mathbf{b}$. In practice the circles drawn through the estimated distances may not always intersect, leaving them separate or completely contained within each other, as illustrated in Fig. 4. In such cases, adjustments to the radius are necessary to ensure intersection. This is achieved by proportionally increasing or decreasing the radius until an intersection is obtained [31].

2) Angulation: Two algorithms that can be employed to determine the location of a BLE tag using AoA are trigonometry, which utilizes the angles and distance between the anchor and the transmitter, and triangulation. Azimuth and elevation angles define the BLE tag projections onto the 2D planes, as illustrated in Fig. 2. Through trigonometry, the target coordinates can be calculated using the estimated distance $\hat{d}_n$, along with the azimuth angle θ_n (in rad), between the n-th anchor and the tag. Considering the projection of the BLE tag in xy-plane with the origin $\begin{bmatrix} 0 & 0 \end{bmatrix}^T$ as the center of the anchor, the coordinates x_{tag} and y_{tag} can be estimated as:

$$\hat{x}_{\text{tag}} = \hat{d}_n \sin(\pi/2 - \theta_n) \tag{8}$$

$$\hat{y}_{\text{tag}} = \hat{d}_n \cos(\pi/2 - \theta_n). \tag{9}$$

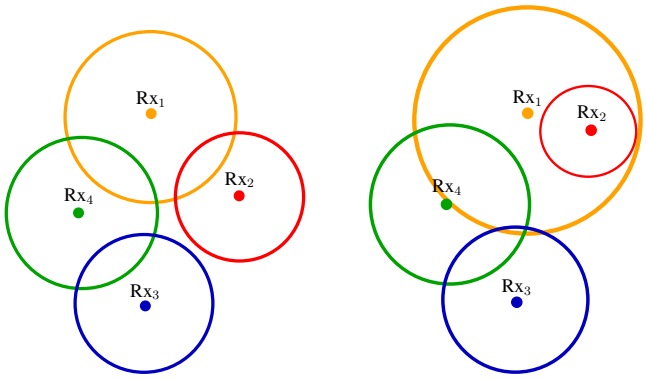

(a) Circles separated. (b) Circle within another circle.

Fig. 4: Example of multilateration non-intersecting circles.

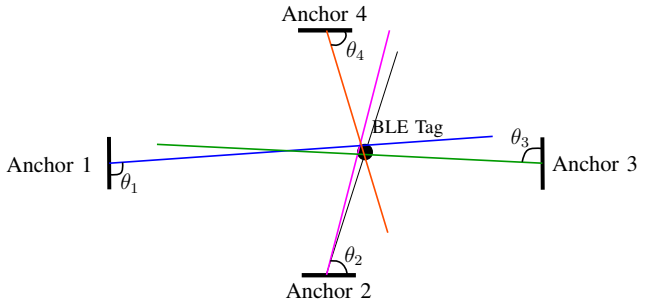

Fig. 5: Location of the BLE tag is estimated through the intersection of the straight lines formed by the detected AoAs.

The estimated position is given by:

$$\hat{\mathbf{p}}_{\text{A+D}} = \begin{bmatrix} \bar{\hat{x}}_{\text{tag}} & \bar{\hat{y}}_{\text{tag}} \end{bmatrix}^T, \tag{10}$$

where $\bar{\hat{x}}_{\text{tag}}$ and $\bar{\hat{y}}_{\text{tag}}$ are the mean of the estimated coordinates obtained from (8) and (9) for N anchors. This method is referred to as "AoA+RSSI" trigonometry.

In triangulation, location is estimated by creating and extending the lines of sight established from measurements of multiple anchors; such a technique can pinpoint the target location at the point of intersection [32], [33], as illustrated in Fig. 5. The azimuth angle formed between the n-th BLE anchor and BLE tag can be calculated by:

$$\theta_n = \arctan\left(\frac{y_n - y_{\text{tag}}}{x_n - x_{\text{tag}}}\right). \tag{11}$$

Rearranging (11) for a set of N BLE anchors:

$$\begin{aligned} y_1 - x_1\tan(\theta_1) &= y_{\text{tag}} - x_{\text{tag}}\tan(\theta_1), \\ y_2 - x_2\tan(\theta_2) &= y_{\text{tag}} - x_{\text{tag}}\tan(\theta_2), \\ &\vdots \\ y_N - x_N\tan(\theta_N) &= y_{\text{tag}} - x_{\text{tag}}\tan(\theta_N). \end{aligned}$$

This system can be expressed in the form $\mathbf{c} = \mathbf{H}\mathbf{p}$, where

$$\mathbf{H} = \begin{bmatrix} -\tan(\theta_1) & 1 \\ -\tan(\theta_2) & 1 \\ \vdots & \vdots \\ -\tan(\theta_N) & 1 \end{bmatrix}, \tag{12}$$

This article has been accepted for publication in IEEE Internet of Things Journal. This is the author's version which has not been fully edited and content may change prior to final publication. Citation information: DOI 10.1109/JIOT.2025.3530866

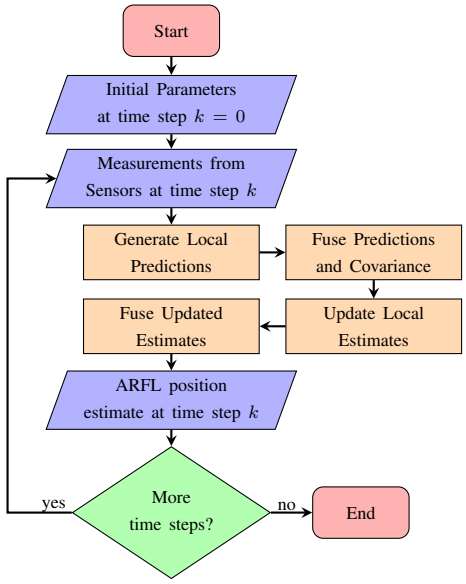

Fig. 6: ARFL Flowchart.

$$\mathbf{c} = \begin{bmatrix} y_1 - x_1 \tan(\theta_1) \\ y_2 - x_2 \tan(\theta_2) \\ \vdots \\ y_N - x_N \tan(\theta_N) \end{bmatrix}, \tag{13}$$

$$\mathbf{p} = \begin{bmatrix} x_{\text{tag}} \\ y_{\text{tag}} \end{bmatrix}. \tag{14}$$

Considering that the azimuth measurements $\{\hat{\theta}_n\}_{n=1}^{N}$ are subject to errors, an estimated position is obtained using the least squares method as:

$$\hat{\mathbf{p}}_{\text{AoA}} = \hat{\mathbf{p}} = (\mathbf{H}^T\mathbf{H})^{-1}\mathbf{H}^T\mathbf{c}, \tag{15}$$

which minimizes $\sum_{n=1}^{N}(\theta_n - \hat{\theta}_n)^2$. We refer to this method as "AoA-only" triangulation.

IV. Proposed Scheme: ARFL

The accuracy of RSSI and AoA is often compromised by noisy measurements, which can be attributed to factors such as multipath effects, signal reflections, refraction, and intrinsic reading errors in devices. Additionally, packet loss due to interference from other radio frequency networks can further reduce reliability. An alternative to mitigate these effects is to employ stochastic filters, which effectively enhance measurement accuracy. Stochastic filtering is a mathematical tool that is used to estimate the state of a system over time in the presence of uncertainty. Among the common stochastic filters available in the literature, in this work we resort to the KF [6] along with sensor fusion [34], [35]. The flowchart of the proposed ARFL scheme is illustrated in Fig. 6.

A. Kalman Filter

The KF minimizes the estimation error of the state of a linear system with Gaussian noise added to the measurements. It operates in two main stages, namely *prediction* and *update*.

In the absence of external control inputs, one can apply KF to BLE IPS through the following discrete-time functions [36]:

$$\mathbf{x}_k = \mathbf{A}\mathbf{x}_{k-1} + \mathbf{w}_{k-1}, \tag{16}$$

$$\mathbf{z}_k = \mathbf{C}\mathbf{x}_k + \mathbf{v}_k, \tag{17}$$

where $\mathbf{x}_k$ and $\mathbf{z}_k$ represent the state and the real measurement vectors at time step k, respectively. Moreover, $\mathbf{A} \in \mathbb{R}^{j_x \times j_x}$ is the state transition matrix, where $j_x \in \mathbb{Z}$ is the number of state variables, and $\mathbf{C} \in \mathbb{R}^{j_z \times j_x}$ is the observation matrix, being $j_z \in \mathbb{Z}$ the number of variables in the measurement vector. The process noise is represented by $\mathbf{w}_{k-1} \in \mathbb{R}^{j_x \times 1} \sim \mathcal{N}(0, \mathbf{Q})$, where the noise covariance matrix of the process is $\mathbf{Q} = q\mathbf{I}_{j_x} \in \mathbb{R}^{j_x \times j_x}$, with $\mathbf{I}_i$ being an $i \times i$ identity matrix and $q \in \mathbb{R}$. The measurement noise is described as $\mathbf{v}_k \in \mathbb{R}^{j_z \times 1} \sim \mathcal{N}(0, \mathbf{R})$, where $\mathbf{R}$ represents the measurement covariance given by $\mathbf{R} = r\mathbf{I}_{j_z} \in \mathbb{R}^{j_z \times j_z}$ and $r \in \mathbb{R}$.

In our model, $\mathbf{x}_k$, $\mathbf{A}$, and $\mathbf{C}$ can be defined as

$$\mathbf{x}_k = \begin{bmatrix} x(k) & v_x(k) & y(k) & v_y(k) \end{bmatrix}^T, \tag{18}$$

$$\mathbf{A} = \begin{bmatrix} 1 & \Delta T & 0 & 0 \\ 0 & 1 & 0 & 0 \\ 0 & 0 & 1 & \Delta T \\ 0 & 0 & 0 & 1 \end{bmatrix}, \tag{19}$$

$$\mathbf{C} = \begin{bmatrix} 1 & 0 & 0 & 0 \\ 0 & 0 & 1 & 0 \end{bmatrix}, \tag{20}$$

where $v_x(k)$ and $v_y(k)$ represent respectively the velocities (m/s) in coordinates $x(k)$ and $y(k)$ at time step k, and ΔT is the sampling time.

1) Prediction: This phase estimates the future state based on the current state estimate and predicts the associated uncertainty of such estimate through the covariance matrix [36]

$$\hat{\mathbf{x}}_{k|k-1} = \mathbf{A}\,\hat{\mathbf{x}}_{k-1|k-1}, \tag{21}$$

$$\mathbf{P}_{k|k-1} = \mathbf{A}\,\mathbf{P}_{k-1|k-1}\,\mathbf{A}^T + \mathbf{Q}, \tag{22}$$

where $\hat{\mathbf{x}}_{k|k-1} \in \mathbb{R}^{4\times 1}$ is the a priori state estimate at time step k give the a posteriori state estimate at time step $k-1$, $\mathbf{P}_{k|k-1} \in \mathbb{R}^{4\times 4}$ is the a priori error covariance matrix that collects the deviation in the estimations at time step k given the a posteriori error covariance matrix at time step $k-1$. The initial values of $\hat{\mathbf{x}}_{0|0}$ and $\mathbf{P}_{0|0}$, *i.e.* for $k = 0$, can be manually assigned before the algorithm starts.

2) Measurement update: At this stage, the predicted state is corrected by incorporating new measurement data. Here, the KF first computes the Kalman Gain $\mathbf{K}_k \in \mathbb{R}^{4\times 2}$ at time step k, which determines the weight given to the new measurement versus the predicted state. Finally, the filter updates both the state estimate and its associated uncertainty as [36]

$$\mathbf{K}_k = \mathbf{P}_{k|k-1}\,\mathbf{C}^T(\mathbf{C}\,\mathbf{P}_{k|k-1}\,\mathbf{C}^T + \mathbf{R})^{-1}, \tag{23}$$

$$\hat{\mathbf{x}}_{k|k} = \hat{\mathbf{x}}_{k|k-1} + \mathbf{K}_k(\mathbf{z}_k - \mathbf{C}\,\hat{\mathbf{x}}_{k|k-1}), \tag{24}$$

$$\mathbf{P}_{k|k} = (\mathbf{I}_4 - \mathbf{K}_k\,\mathbf{C})\mathbf{P}_{k|k-1}, \tag{25}$$

where $\hat{\mathbf{x}}_{k|k}$ and $\mathbf{P}_{k|k}$ are the a posteriori state estimate and error covariance matrix, respectively.

In addition to the potential of KF to reduce noise-induced error, the quality of estimations can also be improved by using sensor fusion. This technique involves gathering information

from the environment through multiple sensors and combining their data, reducing uncertainty compared to relying on individual sensors [37].

B. Sensor Fusion

One of the most well-known fusion techniques is the T2TF [34], where the individual state estimates from different sensors are fused to create a new estimate of the state vector. A derivation of the T2TF is the track fusion model with fused prediction (TFP) [35]. Let us represent as $\hat{\mathbf{x}}^f_{k|k}$ the a posteriori state estimate obtained through KF from the f-th different sensor or technique, with $f \in \{1, 2, \dots F\}$, being F the total number of different fused sensor/techniques. The TFP is adopted in this work to combine the estimates obtained by the aforementioned "AoA+RSSI" and "AoA-only" algorithms. The proposed fusion is referred to as ARFL.

Unlike the single step of T2TF, TFP performs two fusion steps: one for the fused prediction and another for the fused state estimate. First, in local Kalman filtering prediction, two individual filters generate a priori state estimates $\hat{\mathbf{x}}^1_{k|k-1}$ and $\hat{\mathbf{x}}^2_{k|k-1}$ from sensors 1 and 2, as in (21). These estimates are then fused into a combined state prediction $\hat{\mathbf{x}}_{k|k-1}$ as [35]:

$$\hat{\mathbf{x}}_{k|k-1} = \hat{\mathbf{x}}^1_{k|k-1} + \frac{\mathbf{P}^1_{k|k-1}}{\mathbf{P}^1_{k|k-1}+\mathbf{P}^2_{k|k-1}}(\hat{\mathbf{x}}^2_{k|k-1} - \hat{\mathbf{x}}^1_{k|k-1}), \quad (26)$$

where $\mathbf{P}^f_{k|k-1}$, $f \in \{1, 2\}$, is the a priori error covariance matrix for the individual estimate $\hat{\mathbf{x}}^f_{k|k-1}$ of sensor f from (22).

The combined a priori state prediction $\hat{\mathbf{x}}_{k|k-1}$ is used to correct the individual a posteriori state estimates, $\hat{\mathbf{x}}^1_{k|k}$ and $\hat{\mathbf{x}}^2_{k|k}$, at time step k based on their respective measurements $\mathbf{z}^1_k$ and $\mathbf{z}^2_k$. The correction equation can be expressed as [35]:

$$\begin{aligned} \hat{\mathbf{z}}_{k|k-1} &= \mathbf{C}\,\hat{\mathbf{x}}_{k|k-1}, \\ \hat{\mathbf{x}}^f_{k|k} &= \hat{\mathbf{x}}_{k|k-1} + \mathbf{K}^f_k(\mathbf{z}^f_k - \hat{\mathbf{z}}_{k|k-1}), \end{aligned} \quad (27)$$

with $\hat{\mathbf{z}}_{k|k-1}$ being the estimated measurement vector at time step k obtained through the combined a priori state prediction.

The Kalman Gain $\mathbf{K}^f_k$ for each sensor is obtained from (23), where the covariance matrix $\mathbf{P}_{k|k-1}$ is the error covariance matrix of the fused prediction state $\hat{\mathbf{x}}_{k|k-1}$, defined as [35]:

$$\mathbf{P}_{k|k-1} = \mathbf{P}^1_{k|k-1} - \frac{\mathbf{P}^1_{k|k-1}}{\mathbf{P}^1_{k|k-1}+\mathbf{P}^2_{k|k-1}}\mathbf{P}^1_{k|k-1}. \quad (28)$$

Finally, the fused a posteriori estimate $\hat{\mathbf{x}}_{k|k}$ at time step k is obtained by combining local estimates $\hat{\mathbf{x}}^1_{k|k}$ and $\hat{\mathbf{x}}^2_{k|k}$ as [35]:

$$\hat{\mathbf{x}}_{k|k} = \hat{\mathbf{x}}^1_{k|k} + \frac{\mathbf{P}^1_{k|k}}{\mathbf{P}^1_{k|k}+\mathbf{P}^2_{k|k}}(\hat{\mathbf{x}}^2_{k|k} - \hat{\mathbf{x}}^1_{k|k}), \quad (29)$$

where $\mathbf{P}^f_{k|k}$ is the a posteriori covariance matrix for the local estimate $\hat{\mathbf{x}}^f_{k|k}$ of sensor f, obtained from (25).

Although the TFP algorithm is computationally more complex than T2TF, it better mitigates the impact of noise compared to T2TF, due to its additional fusion procedures [35].

Algorithm 1 summarizes the proposed ARFL algorithm. Here, $\hat{\mathbf{p}}^f_k$ represents the estimated positions at time step k; $\mathbf{P}^f_{0|0} \in \mathbb{R}^{4\times4}$ is the initial error covariance matrix, where $f = 1$ represents the "AoA-only" method, while $f = 2$ stands for the "AoA+RSSI" technique; $\mathbf{R}_1 \in \mathbb{R}^{2\times2}$ and $\mathbf{R}_2 \in \mathbb{R}^{2\times2}$ are the measurement covariance matrices for triangulation and trigonometry, respectively. The initial coordinates $x(0)$ and $y(0)$ represent the initial position of the movement, while the initial velocities $v_x(0)$ and $v_y(0)$ are set to zero. Moreover, $\hat{\mathbf{P}}_{\text{ARFL}} \in \mathbb{R}^{4\times K}$ is the output matrix that has the estimated positions for all time steps, and $\hat{\mathbf{P}}_{\text{ARFL}}[:, k]$ represents the k-th column of the matrix $\hat{\mathbf{P}}_{\text{ARFL}}$[1].

Algorithm 1: Proposed ARFL Algorithm

Input: Observation matrix $\mathbf{C}$, noise covariance matrix $\mathbf{Q}$, state transition matrix $\mathbf{A}$, error covariance matrices $\mathbf{P}^1_{0|0}$ and $\mathbf{P}^2_{0|0}$, measurement covariances $\mathbf{R}_1$ and $\mathbf{R}_2$, total number of time steps K, initial position and velocities $x(0)$, $y(0)$, $v_x(0)$, $v_y(0)$.

`/* superscript` $f = 1$ `represents the "AoA-only" method, while` $f = 2$ `stands for the "AoA+RSSI" technique */`

Output: Estimated positions of all steps, $\hat{\mathbf{P}}_{\text{ARFL}}$

begin
- $\mathbf{x}^1_{0|0} = \mathbf{x}^2_{0|0} \leftarrow [x(0) \quad v_x(0) \quad y(0) \quad v_y(0)]^T$; `/* initial state estimate for "AoA-only" and "AoA+RSSI" */`
- **for** $k \leftarrow 1$ **to** K **do** `/* runs through` K `steps */`
  - Obtain $\hat{\mathbf{p}}^1_k = \hat{\mathbf{p}}_{\text{AoA}}$ with Equation (15);
  - Calculate $\hat{\mathbf{p}}^2_k = \hat{\mathbf{p}}_{\text{A+D}}$ from Equation (10);
  - Assign $\mathbf{z}^1_k = \hat{\mathbf{p}}^1_k$ and $\mathbf{z}^2_k = \hat{\mathbf{p}}^2_k$;
  - Obtain local $\hat{\mathbf{x}}^f_{k|k-1}$ from Equation (21);
  - Calculate local $\mathbf{P}^f_{k|k-1}$ from Equation (22);
  - Obtain fused $\hat{\mathbf{x}}_{k|k-1}$ from Equation (26);
  - Calculate fused $\mathbf{P}_{k|k-1}$ from Equation (28);
  - Update local $\mathbf{K}^f_k$ using Equation (23);
  - Update local $\mathbf{P}^f_{k|k}$ with Equation (25);
  - Update local $\hat{\mathbf{x}}^f_{k|k}$ with the aid of Equation (27);
  - Obtain the updated fused $\hat{\mathbf{x}}_{k|k}$ from Equation (29);
  - Save result: $\hat{\mathbf{P}}_{\text{ARFL}}[:, k] \leftarrow \hat{\mathbf{x}}_{k|k}$;
- **end**
- **return** $\hat{\mathbf{P}}_{\text{ARFL}}$; `/* estimated position of all steps */`

end

The presented algorithm differs from the one proposed by [35] in its treatment of the cross-covariance matrix between state estimates. Since both techniques estimate the same process, the two estimates of the same state become correlated due to common process noise [38], resulting in a nonzero cross-covariance matrix, as considered in [35].

Under the assumption of error independence, *i.e.*, that the position estimation errors from different sensors corresponding to the same target are independent, the approach of disregarding the cross-covariance matrix can be adopted [34]. Since position estimates obtained from IPS algorithms are prone to high errors due to measurement noise, neglecting the cross-covariance improves accuracy in ARFL by giving greater weight to the model prediction than to the measurements [39].

V. Results

The performance of our proposed scheme is evaluated with the aid of the dataset provided by [7], which was obtained using a u-blox XPLR-AoA-1 Bluetooth 5.1 kit. The experimental environment is an $14\,\text{m} \times 8\,\text{m}$ indoor space. One anchor was positioned at each corner of the room, at a height of $2.3\,\text{m}$.

[1]Note that, despite the similar notation, this differs from the error covariance matrix introduced in Section IV-A in the scope of Kalman Filtering.

This article has been accepted for publication in IEEE Internet of Things Journal. This is the author's version which has not been fully edited and content may change prior to final publication. Citation information: DOI 10.1109/JIOT.2025.3530866

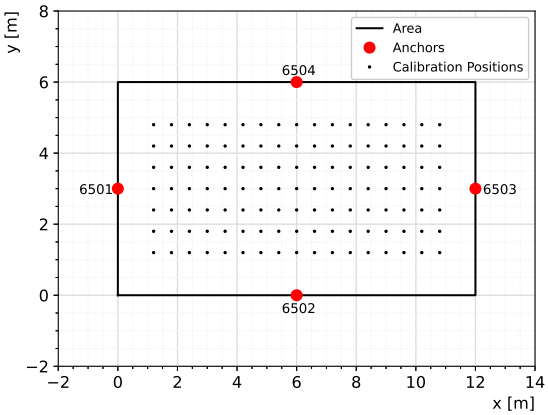

Fig. 7: Calibration scenario.

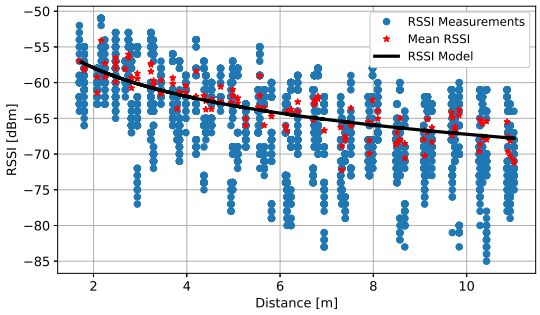

Fig. 8: RSSI behavior for anchor 6501.

Each anchor has the following dataset measurements: RSSI, azimuth angle, elevation angle, target true coordinates, as well as initial and final time. Although our analysis may be limited by the scope, to the best of the authors' knowledge, this is the most comprehensive dataset available for Bluetooth DF.

The dataset was analyzed using Python, and the RSSI and azimuth readings from the three advertised Bluetooth channels (37, 38, and 39) of the calibration and movement scenarios were fed into algorithms that calculate positions using RSSI and AoA techniques. Although [7] includes two different polarizations, we use only the second polarization for RSSI values, as it exhibited more reliable data. Furthermore, the current firmware for the C211 Antenna Array Board no longer reports RSSI from both polarizations [40], suggesting that measurements from the other polarization might be unreliable.

The Python code to reproduce the results is available in [41].

A. Calibration Scenario

The calibration environment described in [7] is depicted in Fig. 7. It consists of a BLE tag placed on a tripod (to reduce human body interference) at a height of $1.1\,\mathrm{m}$ placed at 63 different locations, spaced by $0.60\,\mathrm{m}$. This setup allows us to obtain the PLc α as the first result. Fig. 8 illustrates the behavior of RSSI captured by anchor 6501 and its correlation with distance. In some cases, there is more than one mean value for a given distance because different coordinates are at the same distance from the anchor.

To obtain the PLc, processing was carried out on the RSSI values to remove outliers, identified using the Z-score, which is a measure of how many standard deviations a data point is from the mean of a dataset, calculated as $Z_{\text{score}} = \dfrac{X_{\text{RSSI}} - \mu_{\text{RSSI}}}{\sigma_{\text{RSSI}}}$, where X_{RSSI} denotes the RSSI measurement at a given distance, with mean μ_{RSSI} and standard deviation σ_{RSSI}. Any RSSI data with a Z-score of two or more was discarded. The values of PLc α_n for the n-th anchor, with $n \in \{6501, 6502, 6503, 6504\}$, which minimize the error between the RSSI model and the mean of the measurements, are $\alpha_{6501} = 1.329$, $\alpha_{6502} = 1.852$, $\alpha_{6503} = 1.420$, and $\alpha_{6504} = 2.012$. These differences in the PLc values between anchors can be attributed to the shadowing effects.

B. Movement Scenario

The movement scenarios presented in [7] capture dynamic changes in RSSI and AoA data. The data were collected while a person moved throughout the room at a speed of approximately $0.5\,\mathrm{m/s}$. The PLc values used for distance calculations are those established previously, along with measurements from the same antenna polarization. Three distinct paths (namely Case I, Case II, and Case III) were followed, each repeated four times.

The authors of [7] provide ground truth (GT) data with target coordinates and timestamps for specific positions. To achieve a more continuous trajectory, additional localization points were interpolated by assuming a constant velocity model and calculating the mean velocity between consecutive points. Later in this subsection, we will present the impact of this interpolation on the average error.

1) Case I: The first case refers to the path illustrated by blue dots in Fig. 9. This figure also depicts the path predicted by AoA-only and AoA+RSSI with and without KF, and the ARFL technique for the first repetition. As can be observed, the accuracy is generally higher in the central area of the room. This is due to the smaller angle spread in the anchors, which leads to fewer errors in azimuth angle estimation and, consequently, increases the accuracy of AoA-based methods. In addition, trajectory estimation was also performed using multilateration. The errors between real and estimated positions are presented in Fig. 10, where "MLT" stands for multilateration. The error d_ϵ represents the average distance between true and estimated coordinates for the four repetitions, given by $d_\epsilon = \dfrac{1}{m}\sum_{i=1}^{m}\sqrt{(x_i - \hat{x}_i)^2 + (y_i - \hat{y}_i)^2}$. Here, x_i and y_i are the true coordinates at the i-th position, $\hat{x}_i$ and $\hat{y}_i$ denote the estimated coordinates at the i-th position, and m denotes the number of estimated positions through the test.

Fig. 10 reveals that, among filter-free schemes, AoA-only IPS is the most accurate method. This superiority comes from two key factors. First, triangulation is based solely on the AoA, eliminating the need for RSSI measurements and the PLc. This reduces the errors introduced by the multipath effects in these measurements. Second, the azimuth angle measured by the anchors proves to be a more reliable metric for position estimation than RSSI measurements.

Furthermore, the results show significant improvements in distance accuracy when combining AoA+RSSI compared to

This article has been accepted for publication in IEEE Internet of Things Journal. This is the author's version which has not been fully edited and content may change prior to final publication. Citation information: DOI 10.1109/JIOT.2025.3530866

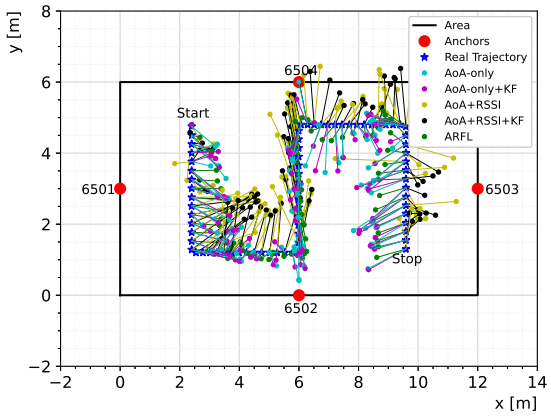

Fig. 9: Position estimates in Case I. The lines represent the error between prediction and actual position.

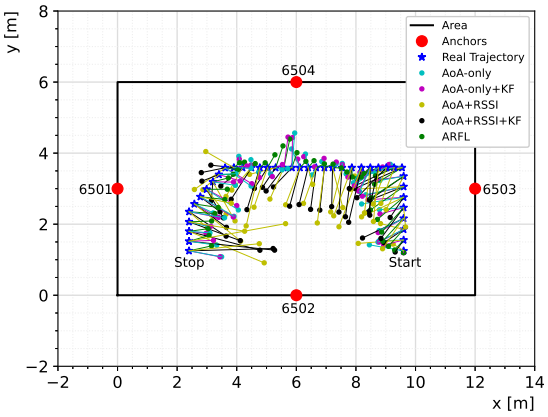

Fig. 11: Position estimates in Case II.

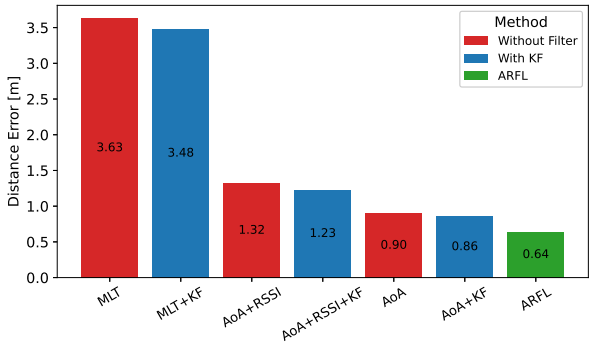

Fig. 10: Bar graph with the distance errors d_ϵ for Case I.

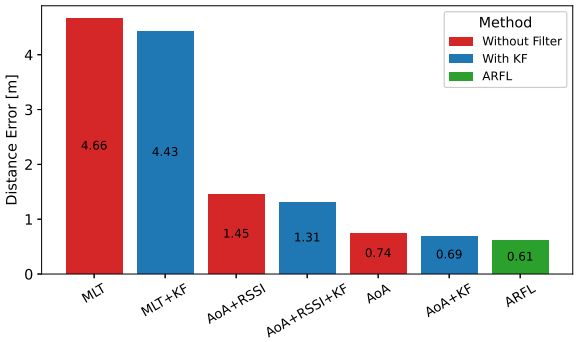

Fig. 12: Bar graph with the distance errors d_ϵ for Case II.

RSSI multilateration only. AoA+RSSI improves accuracy in 63.63%. In particular, AoA-only positioning outperforms both the multilateration and AoA+RSSI methods by a substantial margin, achieving 75.20% and 31.82% improvements in precision, respectively. These findings strongly suggest that AoA positioning offers superior accuracy for indoor localization tasks. The influence of the KF on the estimated positions is also evident in the results, representing an average improvement of 5.13% compared to the unfiltered results.

The proposed ARFL method enhances performance even further, yielding a distance error of $0.64\,\mathrm{m}$, representing an improvement in accuracy compared to other methods with KF applied: 81.61% better than multilateration, 47.97% better than AoA+RSSI, and 25.58% better than AoA-only positioning.

2) Case II: Following a similar methodology as that of Case I, Case II presents a distinct trajectory, as illustrated in Fig. 11. This figure shows both the real path and the path predicted by the ARFL, AoA-only, and AoA+RSSI algorithms, with and without KF, for the first repetition. The corresponding distance errors d_ϵ are presented in Fig. 12.

Consistent with the findings of Case I, Case II reveals that, disregarding the fusion and KF algorithms, AoA-only positioning is the most accurate method. Furthermore, the KF leads to a mean improvement of 7.03% in results. Interestingly, AoA-only position estimation in Case II demonstrates an improvement of 18.27% in accuracy compared to the same algorithm in Case I. A possible reason for this enhancement is that movement occurs in a more central area of the room, resulting in a smaller azimuth angle spread and, consequently, increased accuracy. The RSSI-based method performed worse in this scenario compared to the previous one, but employing AoA with RSSI in the trigonometry method improved accuracy by 68.92% compared to multilateration, a significant enhancement similar to Case I (63.76%).

ARFL provides increased accuracy (11.59%) compared to the AoA+KF method. This is smaller than the improvement observed in Case I (25.58%). The difference can be attributed to the inherent accuracy of the AoA method itself. In Case II, the AoA method yielded a position estimate with relatively low error, leaving less room for significant improvement through fusion with the error-prone AoA+RSSI method. As a result, the sensor fusion result aligns more closely with the more accurate AoA-only positioning.

3) Case III: This case introduces a unique characteristic compared to the previous cases. In addition to movement, the person performing the data collection briefly stopped for one minute at four designated positions: $\begin{bmatrix}240 & 360\end{bmatrix}^T$, $\begin{bmatrix}360 & 120\end{bmatrix}^T$, $\begin{bmatrix}720 & 480\end{bmatrix}^T$, and $\begin{bmatrix}960 & 360\end{bmatrix}^T$.

The remaining data processing pipeline and algorithms employed in Case III follow the same logic as those used in Cases I and II. Fig. 13 presents the real path and the path predicted by the positioning algorithms. The corresponding distance errors are shown in Fig. 14.

Case III highlights a limitation of the prediction algorithm at stopping points, leading to lower accuracy in Case III

This article has been accepted for publication in IEEE Internet of Things Journal. This is the author's version which has not been fully edited and content may change prior to final publication. Citation information: DOI 10.1109/JIOT.2025.3530866

TABLE II: Percentile of the error [m], for Cases I, II and III.

Algorithm	Case I						Case II						Case III					
	5th	25th	50th	75th	95th	Mean	5th	25th	50th	75th	95th	Mean	5th	25th	50th	75th	95th	Mean
MLT	1.99	2.28	3.40	4.70	6.98	**3.63**	1.60	3.50	4.78	5.84	7.48	**4.66**	0.99	2.22	3.16	4.10	5.36	**3.22**
MLT+KF	0.92	2.20	3.07	4.53	7.09	**3.48**	0.73	3.45	4.50	5.96	6.78	**4.43**	1.02	2.19	3.04	3.99	5.18	**3.09**
AoA+RSSI	0.44	0.83	1.28	1.69	2.40	**1.32**	0.49	0.97	1.30	1.84	2.74	**1.45**	0.42	0.88	1.31	1.69	2.12	**1.30**
AoA+RSSI+KF	0.35	0.78	1.24	1.59	2.33	**1.23**	0.44	0.86	1.18	1.55	2.58	**1.31**	0.39	0.86	1.27	1.64	1.99	**1.25**
AoA	0.18	0.45	0.83	1.25	1.78	**0.90**	0.15	0.41	0.74	0.96	1.39	**0.74**	0.23	0.64	0.98	2.08	3.09	**1.33**
AoA+KF	0.16	0.42	0.82	1.21	1.71	**0.86**	0.11	0.38	0.70	0.90	1.31	**0.69**	0.23	0.63	0.96	2.06	3.07	**1.32**
Proposed ARFL	0.13	0.33	0.56	0.97	1.28	**0.64**	0.18	0.35	0.57	0.82	1.09	**0.61**	0.23	0.53	0.93	1.94	2.78	**1.22**

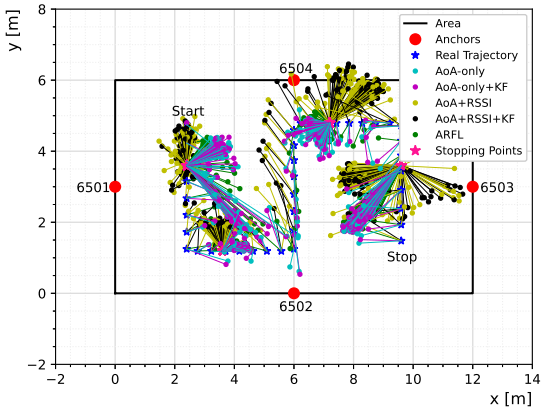

Fig. 13: Position estimates in Case III.

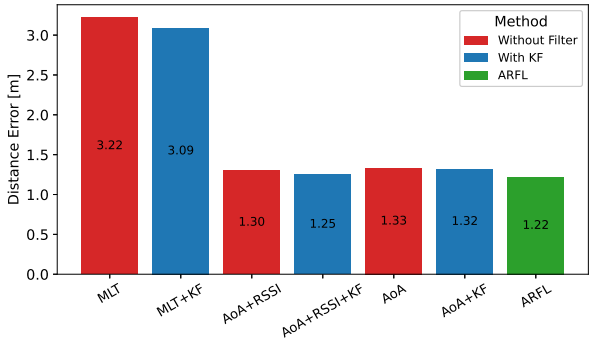

Fig. 14: Bar graph with the distance errors d_ϵ for Case III.

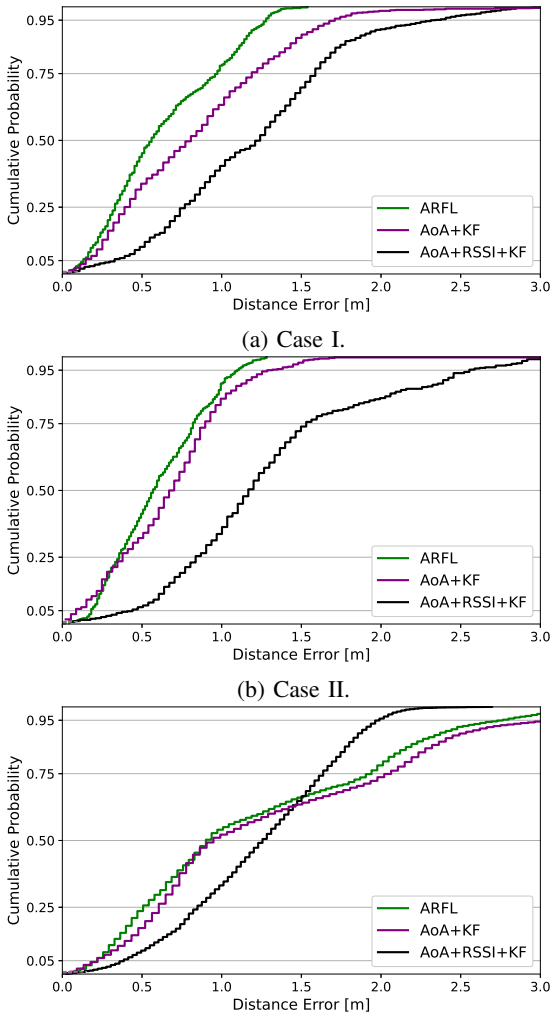

(a) Case I.

(b) Case II.

(c) Case III.

Fig. 15: CDF of the distance errors considering the movement scenarios from (a) Case I, (b) Case II and (c) Case III.

compared to continuously moving scenarios. Moreover, the heatmap from [7, Fig. 8] shows azimuth angle errors, nearing 20°, especially at anchors 6502 and 6504, affecting AoA-based results since 80% of test time occurs at these points.

Despite this challenge, AoA-based positioning remains the most effective method than relying only on RSSI, including during the stops. Sensor fusion also demonstrates its ability to improve the final result, although to a lesser extent compared to the dynamic scenarios of Cases I and II.

As a remark, since the KF model presented in Section IV-A is designed for constant velocity movement and Case III includes a large volume of data collected during static periods, the filter effectiveness is reduced.

The summarized results for all three cases are shown in Table II, and the Cumulative Distribution Function (CDF) is presented in Fig. 15. For Cases I and II, the ARFL consistently demonstrates lower errors across most percentiles, except for a slightly higher error at the 5th percentile in Case II compared to AoA+KF. In Case III, ARFL outperforms up to about the 65th percentile, after which AoA+RSSI+KF yields smaller errors, although ARFL maintains a lower mean error.

Notably, AoA+RSSI+KF exhibits consistent performance across all cases, while the larger angle errors in Case III mostly affect the AoA-only+KF algorithm. Since we designed the KF covariance matrices to give greater weight to AoA-only

over AoA+RSSI measurements, the ARFL results align more closely with AoA-only+KF in this instance.

Another discussion examines measurements across BLE channels. While previous results combined RSSI and AoA data from all channels, we also analyzed positioning errors for each channel individually. RSSI shows greater variation between channels, while AoA remains relatively constant. Consequently, multilateration exhibits more pronounced error differences across channels, whereas AoA-only and AoA+RSSI methods yield more stable results. The use of two AoA-based methods in ARFL allows this fusion to achieve consistent performance across all BLE channel configurations.

Finally, regarding the interpolated points, the approach adopted in our work yields similar results when the error is computed only with the original GT from [7]. For Case I and Case III, ARFL achieves a reduction in average error of $0.05\,\mathrm{m}$ and $0.01\,\mathrm{m}$, respectively. In Case II, d_ϵ increases by $0.01\,\mathrm{m}$.

C. Comparison with Other Fusion Models

We also implemented a Modified Track Fusion (MTF) [35], T2TF [34], and Covariance Intersection (CI) [42] to compare the accuracy of these fusion models with the proposed scheme, given the same system model. When dealing with nonlinear system models and filters, such as the Unscented Kalman Filter (UKF), the observation models differ when using a UKF with only AoA measurements compared to a UKF with both AoA and RSSI measurements. This results in a heterogeneous fusion process, which makes evaluating the covariance matrix more challenging [43]. Moreover, UKF can produce non-positive semi-definite covariance matrices, as demonstrated in [44], which can deteriorate the performance of the fusion algorithms. In any case, the ARFL is compared with the CI fusion using UKF. The results are summarized in Table III.

As shown, ARFL outperforms all schemes in Case I. In Case II, ARFL outperforms the other KF fusion models, showing only a slightly higher mean error than the CI fusion with UKF. Despite the azimuth errors in Case III, which uniquely also includes stopping points, the relative performance between ARFL and most fusion models is similar to that in Case II. This comparison demonstrates that the ARFL schema can be effectively applied in systems requiring high accuracy and low computational load, performing comparably to, or even better than, more complex nonlinear filters and fusion methods. Also, the use of UKF adds more complexity and computational cost than the KF methods [45].

D. Challenges

Deploying Bluetooth 5.1 antennas for indoor positioning requires careful planning, including proper antenna orientation, optimal height to reduce shadowing, and addressing non-line-of-sight conditions by using additional anchors to mitigate multipath effects. Configuring beacon rate, transmit power, and adapting to environmental factors are also crucial. Although ARFL improves accuracy, challenges such as network interference and infrastructure limitations can be also mitigated by adding more anchors, adjusting the BLE setup to the environment, and integrating Inertial Measurement Units (IMUs) to enhance Kalman filter accuracy. Both ARFL and Kalman filter have low processing requirements, making them suitable for a regular Personal Computer (PC).

VI. Conclusion

In this work, we proposed a hybrid indoor positioning system that combines RSSI and AoA measurements through sensor fusion using Kalman Filters, demonstrating improved accuracy over other approaches. The proposed ARFL method was validated with the aid of a public-available Bluetooth 5.1 dataset, showing robustness in indoor environments affected by multipath and interference. For future work, we plan to conduct our own evaluation and produce a dataset for larger and dynamic environments, integrate IMUs, vary the number of anchors and the antennas positioning and orientation to verify the impact on accuracy, and explore the integration of machine learning for further optimization. Key use cases include healthcare, retail, warehousing, and manufacturing, where precise indoor localization can significantly enhance operational efficiency and safety.

References

[1] X. Guo, N. Ansari, F. Hu, Y. Shao, N. R. Elikplim, and L. Li, "A Survey on Fusion-Based Indoor Positioning," *IEEE Commun. Surveys Tuts.*, vol. 22, no. 1, pp. 566–594, Nov. 2020, doi: 10.1109/COMST.2019.2951036.

[2] J. A. López-Pastor, A. J. Ruiz-Ruiz, A. S. Martínez-Sala, and J. Luis Gómez-Tornero, "Evaluation of an indoor positioning system for added-value services in a mall," in *2019 Int. Conf. on Indoor Positioning and Indoor Navig. (IPIN)*, Nov. 2019, pp. 1–8, doi: 10.1109/IPIN.2019.8911822.

[3] K. Casareo and Z. Chaczko, "Beacon-Based Localization Middleware for Tracking in Medical and Healthcare Environments," in *2018 12th Int. Symp. on Med. Inf. and Commun. Technol. (ISMICT)*, Dec. 2018, pp. 1–6, doi: 10.1109/ISMICT.2018.8573701.

[4] P. S. Farahsari, A. Farahzadi, J. Rezazadeh, and A. Bagheri, "A Survey on Indoor Positioning Systems for IoT-Based Applications," *IEEE Internet Things J.*, vol. 9, pp. 7680–7699, Feb. 2022, doi: 10.1109/JIOT.2022.3149048.

[5] K. Lam, "Bluetooth 5.1 Direction Finding: Theory and Practice," Bluetooth Special Interest Group (SIG), Tech. Rep., May 2019. [Online]. Available: https://tinyurl.com/lam2019DF

[6] R. E. Kalman, "A New Approach to Linear Filtering and Prediction Problems," *Trans. of the ASME – J. of Basic Eng.*, vol. 82, no. Series D, pp. 35–45, 1960, doi: 10.1115/1.3662552.

[7] M. Girolami, F. Furfari, P. Barsocchi, and F. Mavilia, "A Bluetooth 5.1 Dataset Based on Angle of Arrival and RSS for Indoor Localization," *IEEE Access*, vol. 11, pp. 81 763–81 776, Aug. 2023, doi: 10.1109/ACCESS.2023.3301126.

[8] M. Girolami, F. Mavilia, F. Furfari, and P. Barsocchi, "An Experimental Evaluation Based on Direction Finding Specification for Indoor Localization and Proximity Detection," *IEEE J. Indoor Seamless Positioning Navig.*, vol. 2, pp. 36–50, Dec. 2023, doi: 10.1109/JISPIN.2023.3345268.

[9] F. Furfari, P. Barsocchi, M. Girolami, and F. Mavilia, "Modelling the Localization Error of an AoA-based Localization System," in *2023 19th Int. Conf. on Intell. Environ. (IE)*, July 2023, pp. 1–4, doi: 10.1109/IE57519.2023.10179094.

[10] P. Sambu and M. Won, "An Experimental Study on Direction Finding of Bluetooth 5.1: Indoor vs Outdoor," in *2022 IEEE Wireless Commun. and Netw. Conf. (WCNC)*, May 2022, pp. 1934–1939, doi: 10.1109/WCNC51071.2022.9771930.

[11] H. Ye, B. Yang, Z. Long, and C. Dai, "A Method of Indoor Positioning by Signal Fitting and PDDA Algorithm Using BLE AOA Device," *IEEE Sensors J.*, vol. 22, no. 8, pp. 7877–7887, Jan. 2022, doi: 10.1109/JSEN.2022.3141739.

[12] Z. Wu, Y. Wang, and J. Fu, "A hybrid RSSI and AoA indoor positioning approach with adapted confidence evaluator," *Ad Hoc Netw.*, vol. 154, p. 103375, Dec. 2023, doi: 10.1016/j.adhoc.2023.103375.

TABLE III: Comparison of percentile of the error [m], for other fusion models.

Algorithm	Case I						Case II						Case III					
	5th	25th	50th	75th	95th	Mean	5th	25th	50th	75th	95th	Mean	5th	25th	50th	75th	95th	Mean
T2TF (KF)	0.14	0.35	0.68	1.10	1.51	**0.75**	0.14	0.45	0.71	0.97	1.37	**0.73**	0.21	0.54	0.95	1.84	2.71	**1.19**
MTF (KF)	0.15	0.35	0.59	1.06	1.36	**0.69**	0.14	0.39	0.61	0.89	1.21	**0.64**	0.23	0.53	0.92	1.93	2.82	**1.22**
CI (KF)	0.16	0.42	0.80	1.20	1.70	**0.85**	0.11	0.39	0.69	0.91	1.32	**0.69**	0.23	0.62	0.96	2.06	3.05	**1.31**
CI (UKF)	0.12	0.41	0.75	1.23	1.51	**0.80**	0.14	0.31	0.51	0.84	1.25	**0.59**	0.34	0.76	1.09	1.56	2.07	**1.18**
Proposed ARFL	0.13	0.33	0.56	0.97	1.28	**0.64**	0.18	0.35	0.57	0.82	1.09	**0.61**	0.23	0.53	0.93	1.94	2.78	**1.22**

[13] S. Monfared, T.-H. Nguyen, L. Petrillo, P. De Doncker, and F. Horlin, "Experimental Demonstration of BLE Transmitter Positioning Based on AOA Estimation," in *2018 IEEE 29th Annu. Int. Symp. on Pers., Indoor and Mobile Radio Commun. (PIMRC)*, Sept. 2018, pp. 856–859, doi: 10.1109/PIMRC.2018.8580796.

[14] M. Girolami, F. Furfari, P. Barsocchi, and F. Mavilia, "A Bluetooth 5.1 Dataset Based on Angle of Arrival and RSS for Indoor Localization," Mar. 2023, doi: 10.5281/zenodo.7759557.

[15] N. I. Piazzese, M. Perrone, and D. P. Pau, "Dataset for Bluetooth 5.1 Direction of Arrival with non Uniform Rectangular Arrays," *Data in Brief*, vol. 39, p. 107576, Dec. 2021, doi: 10.1016/j.dib.2021.107576.

[16] G. Maus, H. Pörner, R. Ahrens, and D. Brückmann, "A Phase Normalization Scheme for Angle of Arrival based Bluetooth Indoor Localization," in *2022 IEEE 65th Int. Midwest Symp. on Circuits and Syst. (MWSCAS)*, Aug. 2022, pp. 1–5, doi: 10.1109/MWSCAS54063.2022.9859290.

[17] G. Maus, "Bluetooth 5.1 Angle of Arrival based Indoor Localization," Oct. 2021, doi: 10.21227/2j4h-3w77.

[18] u-blox, "XPLR-AOA-1: Bluetooth 5.1 direction finding explorer kit with NINA-B4," 2024. [Online]. Available: https://tinyurl.com/XPLR-AoA-PS

[19] M. Ji, J. Kim, J. Jeon, and Y. Cho, "Analysis of positioning accuracy corresponding to the number of BLE beacons in indoor positioning system," in *2015 17th Int. Conf. on Advanced Commun. Technol. (ICACT)*, July 2015, pp. 92–95, doi: 10.1109/ICACT.2015.7224764.

[20] I. Gouzouasis, S. Papaharalabos, M. A. Nasa, and P. Karlsson, "A Novel Antenna System for Direction Finding Applications Using BLE 5.1 Technology," in *2023 17th Eur. Conf. on Antennas and Propag. (EuCAP)*, Mar. 2023, pp. 1–5, doi: 10.23919/EuCAP57121.2023.10132951.

[21] N. Pakanon, M. Chamchoy, and P. Supanakoon, "Study on Accuracy of Trilateration Method for Indoor Positioning with BLE Beacons," in *2020 6th Int. Conf. on Eng., Appl. Sci. and Technol. (ICEAST)*, July 2020, pp. 1–4, doi: 10.1109/ICEAST50382.2020.9165464.

[22] A. C. Eyng, O. K. Rayel, E. Oroski, and J. L. Rebelatto, "Kalman Filtering-Aided Hybrid Indoor Positioning System With Fingerprinting And Multilateration," in *2020 IEEE 91st Veh. Technol. Conf. (VTC2020-Spring)*. Antwerp, Belgium: IEEE, May 2020, pp. 1–5, doi: 10.1109/VTC2020-Spring48590.2020.9129422.

[23] M. Salimibeni and A. Mohammadi, "RL-IFF: Indoor Localization via Reinforcement Learning-Based Information Fusion," in *ICASSP 2023 - 2023 IEEE Int. Conf. on Acoust., Speech and Signal Process. (ICASSP)*. Rhodes Island, Greece: IEEE, June 2023, pp. 1–5, doi: 10.1109/ICASSP49357.2023.10094935.

[24] N. Paulino, L. M. Pessoa, A. Branquinho, and E. Goncalves, "Evaluating a Novel Bluetooth 5.1 AoA Approach for Low-Cost Indoor Vehicle Tracking via Simulation," in *2021 Joint Eur. Conf. on Netw. and Commun. & 6G Summit (EuCNC/6G Summit)*. Porto, Portugal: IEEE, June 2021, pp. 259–264, doi: 10.1109/EuCNC/6GSummit51104.2021.9482525.

[25] F. A. Toasa, L. Tello-Oquendo, C. R. Peñafiel-Ojeda, and G. Cuzco, "Experimental Demonstration for Indoor Localization Based on AoA of Bluetooth 5.1 Using Software Defined Radio," in *2021 IEEE 18th Annu. Consum. Commun. & Netw. Conf. (CCNC)*, Jan. 2021, pp. 1–4, doi: 10.1109/CCNC49032.2021.9369638.

[26] G. Pau, F. Arena, Y. E. Gebremariam, and I. You, "Bluetooth 5.1: An Analysis of Direction Finding Capability for High-Precision Location Services," *Sensors*, vol. 21, no. 11, p. 3589, Jan. 2021, doi: 10.3390/s21113589.

[27] u-blox, "XPLR-AOA-1 and XPLR-AOA-2 explorer kits," Feb. 2024. [Online]. Available: https://tinyurl.com/XPLR-AOA-US

[28] H. Kwasme and S. Ekin, "Rssi-based localization using lorawan technology," *IEEE Access*, vol. 7, pp. 99 856–99 866, July 2019, doi: 10.1109/ACCESS.2019.2929212.

[29] A. Goldsmith, *Wireless Communications*. Cambridge University Press, 2005, doi: 10.1017/CBO97805118412248.

[30] J. Koo and H. Cha, "Localizing WiFi Access Points Using Signal Strength," *IEEE Commun. Lett.*, vol. 15, no. 2, pp. 187–189, Dec. 2011, doi: 10.1109/LCOMM.2011.121410.101379.

[31] Y. You and C. Wu, "Indoor Positioning System With Cellular Network Assistance Based on Received Signal Strength Indication of Beacon," *IEEE Access*, vol. 8, pp. 6691–6703, Dec. 2020, doi: 10.1109/ACCESS.2019.2963099.

[32] G. Ottoy and L. De Strycker, "An Improved 2D Triangulation Algorithm for Use With Linear Arrays," *IEEE Sensors J.*, vol. 16, no. 23, pp. 8238–8243, June 2016, doi: 10.1109/JSEN.2016.2584647.

[33] A. Küpper, *Location-Based Services: Fundamentals and Operation*. John Wiley & Sons, Ltd, Aug. 2005, doi: 10.1002/0470092335.

[34] Y. Bar-Shalom and L. Campo, "The Effect of the Common Process Noise on the Two-Sensor Fused-Track Covariance," *IEEE Trans. Aerosp. Electron. Syst.*, vol. AES-22, no. 6, pp. 803–805, Nov. 1986, doi: 10.1109/TAES.1986.310815.

[35] J. Gao and C. Harris, "Some remarks on Kalman filters for the multisensor fusion," *Inf. Fusion*, vol. 3, no. 3, pp. 191–201, Sept. 2002, doi: 10.1016/S1566-2535(02)00070-2.

[36] A. Belmonte-Hernández, G. Hernández-Peñaloza, F. Álvarez, and G. Conti, "Adaptive Fingerprinting in Multi-Sensor Fusion for Accurate Indoor Tracking," *IEEE Sensors J.*, vol. 17, no. 15, pp. 4983–4998, June 2017, doi: 10.1109/JSEN.2017.2715978.

[37] A. Assa and F. Janabi-Sharifi, "A Kalman Filter-Based Framework for Enhanced Sensor Fusion," *IEEE Sensors J.*, vol. 15, no. 6, pp. 3281–3292, Jan. 2015, doi: 10.1109/JSEN.2014.2388153.

[38] R. Forsling, B. Noack, and G. Hendeby, "A Quarter Century of Covariance Intersection: Correlations Still Unknown? [Lecture Notes]," *IEEE Control Syst. Mag.*, vol. 44, no. 2, pp. 81–105, Mar. 2024, doi: 10.1109/MCS.2024.3358658.

[39] R. Forsling, "The Dark Side of Decentralized Target Tracking : Unknown Correlations and Communication Constraints," Ph.D. dissertation, Dept. of Elect. Eng., Autom. Control. Linköping Univ., Fac. of Sci. & Eng., Dec. 2023, doi: 10.3384/9789180754101.

[40] u-blox, "u-connectLocate v1.2.0 for NINA-B41," 2022. [Online]. Available: https://tinyurl.com/3unuktts

[41] A. Fabris, O. K. Rayel, J. L. Rebelatto, G. L. Moritz, and R. D. Souza, "AoA and RSSI-Based BLE Indoor Positioning System with Kalman Filter and Data Fusion," Nov. 2024. [Online]. Available: https://doi.org/10.5281/zenodo.14078963

[42] S. Julier and J. Uhlmann, "A Non-divergent Estimation Algorithm n the Presence of Unknown Correlations," in *Proc. 1997 American Control Conf.*, vol. 4, June 1997, pp. 2369–2373 vol.4, doi: 10.1109/ACC.1997.609105.

[43] T. Yuan, Y. Bar-Shalom, and X. Tian, "Heterogeneous track-to-track fusion," in *14th Int. Conf. on Inf. Fusion*, July 2011, pp. 1–8.

[44] S. Julier, J. Uhlmann, and H. Durrant-Whyte, "A New Method for the Nonlinear Transformation of Means and Covariances in Filters and Estimators," *IEEE Trans. on Automatic Control*, vol. 45, no. 3, pp. 477–482, March 2000, doi: 10.1109/9.847726.

[45] C. Urrea and R. Agramonte, "Kalman Filter: Historical Overview and Review of Its Use in Robotics 60 Years after Its Creation," *J. of Sensors*, vol. 2021, no. 1, p. 9674015, Sept. 2021, doi: 10.1155/2021/9674015.